Journal of the Meteorological Society of Japan, Vol. 76, No. 2, pp. 289–305, 1998

Tropical Precipitation Patterns in Response to a Local Warm SST Area Placed at the Equator of an Aqua Planet

By Masahiro Hosaka

Climate Research Department, Meteorological Research Institute, Japan Meteorological Agency

Masaki Ishiwatari

Graduate School of Environmental Earth Science, Hokkaido University

Shin-ichi Takehiro, Kensuke Nakajima

Department of Earth and Planetary Sciences, Faculty of Science, Kyushu University

and

Yoshi-Yuki Hayashi

Graduate School of Mathematical Sciences, University of Tokyo

(Manuscript received 25 July 1997, in revised form 4 February 1998)

Abstract

Aqua planet experiments are performed in order to investigate the effects of an equatorial warm sea surface temperature (SST) area on the tropical large-scale precipitation patterns. The numerical model utilized is a spherical three-dimensional primitive system with resolution of T42L16 and with simplified hydrological processes. The warm SST area is placed at the equator of an aqua planet whose basic SST distribution is zonally uniform and symmetric about the equator.

The calculated tropical precipitation distributions are characterized by the appearance of an east–west asymmetry; precipitation decreases to the west of the warm SST area, while it increases in the longitudinally wide area to the east. The east–west asymmetry appears regardless of the cumulus parameterization schemes utilized (the convective adjustment scheme and the Kuo scheme). In the western region to the warm SST area, an increase of the stability due to a temperature rise in the middle layer is observed and correspondingly downward flow is recognized. These are consistent with the decrease of precipitation. In the eastern region, although a temperature rise appears in the middle layer, the stability decreases due to the increase of water vapor in the lower layer caused by the meridional moisture convergence. This destabilization is consistent with the increase of precipitation.

Experiments in which the wind velocity used in the evaluation of the surface evaporation is fixed are performed to show that WISHE (Wind Induced Surface Heat Exchange) mechanism is not a principal cause for the generation of the east–west asymmetry of the precipitation pattern.

1. Introduction

Investigation of atmospheric circulations realized in an idealistic model system often gives important insights in understanding the complex circulation structures of the real atmosphere. "Aqua planet" experiments have been recognized as one of these investigative tools. An aqua planet model is an idealistic moist atmosphere on a surface covered only with the ocean. Aqua planets have been numerically realized to observe possible characteristics that may be related to the phenomena of the real atmosphere, and may be useful in describing these phenomena.

Hayashi and Sumi (1986) is one of the earliest efforts with aqua planet experiments to investigate

Corresponding author: Masahiro Hosaka, Climate Research Dept. Meteorological Research Institute, Japan Meteorological Agency, 1-1 Nagamine, Tsukuba 305-0052, Japan. E-mail: mhosaka@mri-jma.go.jp

©1998, Meteorological Society of Japan

a possible underlying structure in the precipitation patterns of the tropical atmosphere. They try to reveal idealistic precipitation distributions which would be realized if the SST distribution were fixed and were symmetric about the equator and zonally uniform. Their results indicate that three types of intrinsic precipitation structures may exist in the tropical region; super clusters, Madden-Julian oscillation (MJO or 30–60 day oscillation), and double ITCZs. Numaguti and Hayashi (1991a, b) put forward numerical analyses on the precipitation patterns observed in the aqua planet and show that WISHE (Wind-Induced Surface Heat Exchange) is essential for the existence of MJO, as was originally proposed by Emanuel (1987) and Neelin *et al.* (1987). Numaguti (1993) also reveals that WISHE, combined with the effect of cumulus parameterizations, is crucial for the appearance of the double ITCZ structure.

In the aqua planet studies presented so far, the focus is placed on the precipitation and circulation patterns realized on zonally symmetric boundary conditions. The investigated structures are also zonally symmetric (like ITCZ's) or zonally asymmetric but their amplitudes are zonally uniform (like those of super clusters and MJO). However, the precipitation and circulation patterns observed in the real atmosphere are of course neither zonally symmetric nor uniform; the inhomogeneous boundary conditions such as land-sea distribution and SST distribution cause naturally asymmetric or nonuniform precipitation patterns. However, it is not straightforward to recognize how the inhomogeneity of the boundary conditions cause the observed precipitation and circulation patterns. This is because the amount of precipitation is affected not only by the in situ surface boundary conditions but also by the circulations driven remotely by the distant precipitation (thermal forcing).

With these situations in mind, we will investigate in this paper the precipitation patterns over the entire tropical region caused by a local warm SST area placed at the equator of an aqua planet. On the warm SST area, an intense precipitation activity, a so-called convection center, will emerge. However, we will consider the precipitation patterns all over the tropical region affected by the existence of the convection center; we will not focus on the convection center itself. The SST distribution outside the warm SST area is zonally uniform and symmetric about the equator to minimize the in situ effect on the precipitation properties. In the real atmosphere there are several convection centers located at the Maritime Continent, Africa and South America. The effects of those centers on the global precipitation distribution overlap each other. This situation does not allow us to present a simple explanation on the distribution. In our framework, we hypothetically choose only one of such convection centers and idealize the surface boundary conditions. The resulting nonuniform precipitation patterns will hopefully be simple and easy to understand.

If we can neglect the various feedback mechanisms in the moist atmosphere, the precipitation patterns outside the convection center will be easily predicted. The downward motion should be observed in the neighborhood of the convection center, which should suppress precipitation there. In a non-rotating system, the downward flow will be distributed symmetrically around the warm SST area and so will the dry region. In the tropics, because of the equatorial β effect, the east–west asymmetry will appear in the distributions of the downward flow and the dry region. According to the linear long-wave theory of Gill (1980), the ratio of the extent of the eastern downward flow region to that of the western region will be determined by the propagation speeds of Kelvin and Rossby waves, that is, three to one; and hence, the eastern and western dry regions will be expected to expand by this ratio.

However, we know that it is incomplete to predict the precipitation patterns without considering the water vapor supply and its transport. As for the water vapor supply, Numaguti and Hayashi (1991b), Numaguti (1993) and others show that WISHE plays a crucial role in the determination of the latitudes of ITCZs and in the maintenance of MJO in the zonally symmetric SST problems. In our local warm SST problem, we can again expect that the moisture supply due to evaporation will be enhanced by the low level flow converging into the warm SST area and hence the amount of low level moisture will be increased. The increased moisture will decrease the vertical stability, which will compete with the stabilizing effect by the plausible downward flow around the warm SST area. As for the water vapor transport, the circulation induced by the heating at the convection center should be ruled by the equatorial dynamics, which will cause a certain structure in the vapor transport, resulting in an appearance of a vertically unstable region. In the eastern region to the convection center, for instance, Kelvin wave-like responses associated with surface low pressure are expected to appear. The low level frictional convergence will transport water vapor toward the equatorial low pressure region, which may contribute to the destabilization of that area (*e.g.*, Wang 1988).

We should also consider the existence of the mobile disturbances such as super clusters and MJO, which move eastward. The convection center at the warm SST area may trigger the activity of those disturbances and radiate them to the east. They may contribute to the increase of time mean precipitation in that region.

In the following sections, we will report the re-

sults of our aqua planet experiments with a warm SST area at the equator. In Section 2, we will briefly describe the aqua planet model utilized in this study. In Section 3, the characteristics of the precipitation distributions are summarized by comparing the cases with and without the warm SST area. The detailed consideration on the difference in the precipitation patterns will be presented in Section 4. The cumulus parameterization dependency is checked in Section 5 where the Kuo scheme is used instead of the adjustment scheme. Some discussions will be placed in Section 6. In the present paper, we will focus on the tropical precipitation distribution; the influence on the precipitation and circulation patterns in the subtropics and mid-latitudes will be discussed in a separate paper.

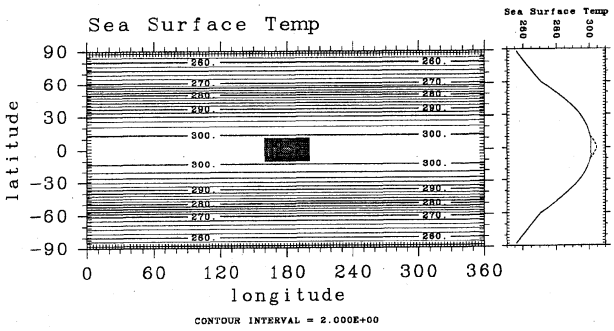

Fig. 1. The distribution of SST used in experiment A4. The local warm SST area is shaded. The figure in the right hand side shows the basic SST distribution (solid line) and the distribution at the longitude 180°, where the value of SST anomaly is the maximum (dashed line).

2. Design of experiments

2.1 The model

The model used in this study is AGCM5 of GFD-DENNOU CLUB edition, which is the three-dimensional primitive system on a sphere (GFD-DENNOU CLUB, 1997). The model is basically the same as that used in Numaguti (1993), and its details are described in Numaguti (1992). The dynamic part is represented by the pseudo spectral method with the triangular truncation at wavenumber 42 (T42) and by the sigma vertical coordinate with 16 vertical levels.

The model contains the following simplified physical processes. The employed cumulus parameterization is the Kuo scheme (Kuo, 1974) or the adjustment scheme (Manabe *et al.*, 1965). The condensed water is removed from the system immediately after condensation and hence there are no clouds. The absorption and scattering of the solar radiation are not included. The longwave absorption is represented by four spectral bands, three of which are of water vapor and one is of dry air. The scattering of the longwave radiation is not included. The absorption coefficients of the longwave radiation are chosen so that the cooling profile of the atmosphere roughly resembles the observed one. The vertical turbulent mixing is represented by the level II scheme of Mellor and Yamada (1974). The surface fluxes of momentum, heat and water vapor are evaluated by the bulk formula.

2.2 Design of experiments

The entire globe is covered with the ocean, whose surface temperature is fixed (time-independent). The experiments with and without the warm SST area are performed and the resultant precipitation patterns are compared.

The basic SST distribution is the same as that used by Numaguti (1993). It is symmetric about the equator and zonally uniform. The value of SST at the equator is 302K and remains constant in the equatorial region between the latitudes of ±7°. The shape of the local warm SST area is rectangular with the longitudinal extent of 40° and the latitudinal extent of 20°. The peak value of SST anomaly is 2, 4, 6 or 8K, and is located at the center of the warm SST area which is placed at the equator. Figure 1 shows the SST distribution with the temperature anomaly whose peak value is 4K. Note that, since grid points do not exist on the equator, the maximum value of the SST anomaly represented in the model is actually 3.4K, which appears at the latitudes of ±1.4°.

The geometry of the warm SST area is empirically chosen to have a convection center which has a single precipitation peak with a fixed location if averaged in the time scale of several tens of days; that is the period of the intraseasonal oscillation. It is desirable that the convection center is steady and its internal structure is simple for the purpose of investigating the precipitation patterns around it. When the warm SST area is too small, the activity of the convection center is weak and its effects on the surroundings become ambiguous, unless the magnitude of the SST anomaly is extremely large. When the warm SST area is too large, multiple convection centers appear in the warm area and interact with each other. The dynamic structure of the convection centers realized on the warm SST area is also an interesting problem, but we do not go into this issue in this paper.

It has been reported that the cumulus parameterization strongly affects the precipitation patterns. In the experiments with the zonally symmetric SST distribution of Numaguti and Hayashi (1991b), the adjustment scheme produces a single ITCZ structure, while the Kuo scheme produces a double ITCZ structure. In this paper, by performing both of the experiments with the adjustment scheme and with the Kuo scheme, we hope to extract possible general

Table 1. The list of the experiments. Δ SST_{max} is the maximum value of the SST anomaly given in each experiment.

Experiments	Δ SST_{max}(K)	Cumulus parameterization	Note
A0	0	Adjustment	
A2	1.7	Adjustment	
A4	3.4	Adjustment	The main experiment
A6	5.1	Adjustment	
A8	6.8	Adjustment	
K0	0	Kuo	
K2	1.7	Kuo	
K4	3.4	Kuo	
K6	5.1	Kuo	
K8	6.8	Kuo	
A0VC	0	Adjustment	No WISHE
A4VC	3.4	Adjustment	No WISHE
K0VC	0	Kuo	No WISHE
K4VC	3.4	Kuo	No WISHE

structures of moist atmospheres independent of the cumulus parameterization. Each experiment is denoted by the combination of A or K, which is the initial of the employed parameterization scheme, and 0, 2, 4, 6 or 8, which is the amount of the SST anomaly at the center of the warm SST area. The experiments performed in this study are listed in Table 1.

In the experiments A0 and K0, the model is integrated from an isothermal rest state and the data from days 700 to 2200 are used for analyses. In the warm SST area experiments of the A series and the K series, the model is integrated from the data at day 700 of A0 and K0, respectively, and the data from days 150 to 900 are used for analyses. The model atmosphere is recognized to reach a quasi-equilibrium state after 150 days of integration. For instance, our experiments show that the position and amplitude of ITCZ adjust to a new state in several tens of days after the change of the SST distribution.

In the following sections, we will focus on the results of the A series. We will present the results of the K series in Section 5 to confirm that the precipitation characteristics obtained in the A series do not depend on the cumulus parameterization.

3. Characteristics of the precipitation patterns

3.1 Precipitation and evaporation without the warm SST area

We first briefly summarize the precipitation and evaporation distributions realized in experiment A0, with which we will later compare the results of the warm SST area experiments. Figure 2 shows the

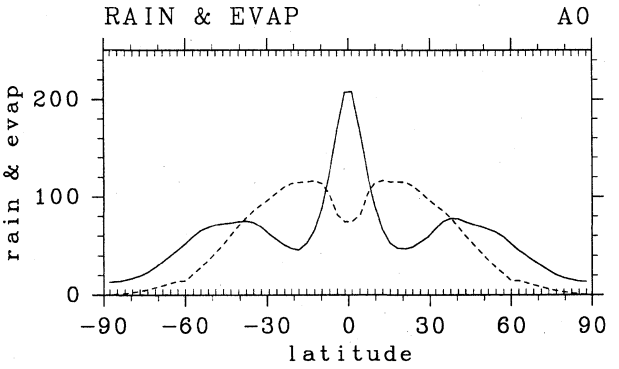

Fig. 2. Latitudinal distributions of the zonal and time mean precipitation (solid line) and evaporation (dashed line) of experiment A0. Unit is W/m^2. Note that 100 W/m^2 corresponds to 3.5 mm/day or 1260 mm/year.

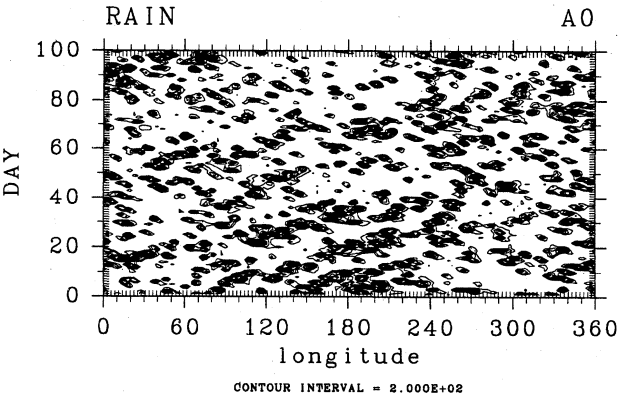

Fig. 3. Temporal evolution of precipitation at the equator of experiment A0. Contour interval is 200 W/m^2. $t = 0$ of the figure is actually day 700 of the experiment.

zonally averaged time mean distributions of precipitation and evaporation for experiment A0. The profile of precipitation has its peak at the equator. The profile of evaporation has maxima in the subtropics and a minimum at the equator. The difference between precipitation and evaporation is accounted for by the meridional water vapor transport which is concentrated in the shallow layer below the level of 900 hPa. Experiment A0 reproduces the zonal mean features of the adjustment experiments reported by Numaguti (1993).

Figure 3 shows the temporal evolution of precipitation at the equator. The eastward propagating grid-scale disturbances (super clusters) are not very coherent, as is reported by Numaguti and Hayashi (1991a, b) on their results of the adjustment experiments. The eastward propagating global structures, which are widely recognized as MJO, are not active, whereas they are clearly seen in the adjustment ex-

periments of Numaguti and Hayashi (1991a, b). We do not go into this difference in this paper[1].

3.2 Precipitation and evaporation with the warm SST area

We will now describe the characteristics of the precipitation patterns obtained in the warm SST area experiments by showing mainly the results of experiment A4. Figure 4a is the time mean horizontal distribution of precipitation for experiment A4, and Fig. 4b is the difference from the zonal mean distribution of experiment A0.

Precipitation over the warm SST area increases greatly and a strong convection center forms. The precipitation maximum of 800 W/m^2 is observed at the center of the warm area. The amount of precipitation averaged over the warm SST area is 250 W/m^2. This exceeds considerably the value 142 W/m^2, which is the amount of precipitation in experiment A0 averaged between the latitudes of $\pm 10°$ (see Table 2). The maximum value of precipitation (800 W/m^2 = 28 mm/day $\sim$ 10000 mm/yr) is comparable to the monthly or seasonal mean values observed at tropical heavy rainfall areas, for example, Indian monsoon regions and Pacific ITCZ regions (*e.g.*, Spencer, 1993).

The notable feature in Fig. 4 is the deformation of ITCZ. There appears an east–west asymmetry in the precipitation distribution at the equator. To the west of the warm SST area, the amount of precipitation decreases in the region with the longitudinal extent of about 70°. To the east of the warm SST area, on the other hand, it increases in the region with the longitudinal extent of about 220°. The precipitation anomaly has its minimum of -100 W/m^2 in the western region at the longitude of 150° and its maximum of $+60$ W/m^2 in the eastern region at the longitudes of 220° and 280°. In the regions along $\pm 10°$ latitudes, the amount of precipitation decreases regardless of the eastern or western sides.

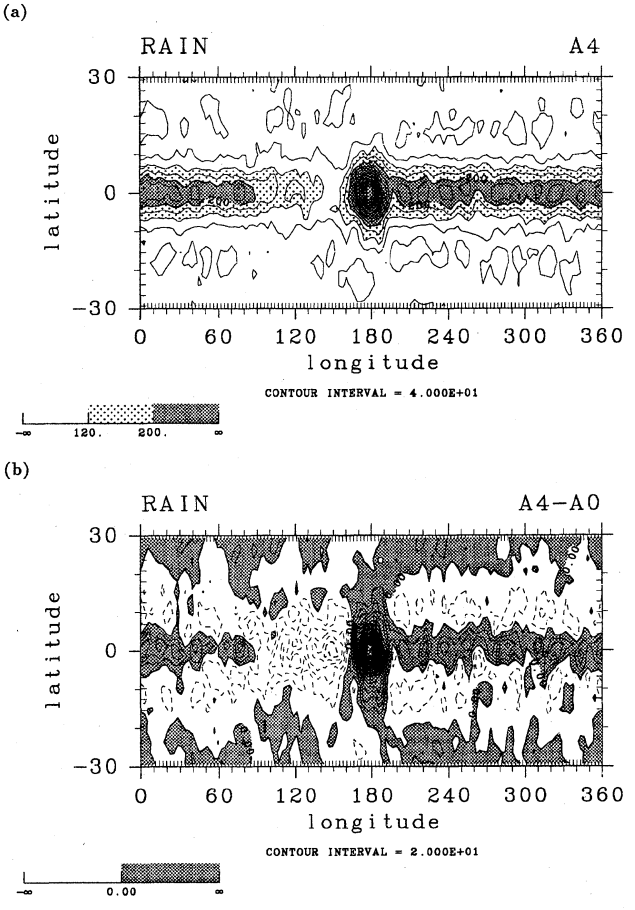

Fig. 4. (a) Time mean horizontal distribution of precipitation for experiment A4. (b) Its difference from the zonal mean distribution of experiment A0. Unit is W/m^2. Contour intervals are (a) 40 W/m^2 and (b) 20 W/m^2.

Precipitation increases only at the longitudes where the warm SST is placed.

As for experiments A2, A6 and A8 we show only the longitudinal distributions of precipitation at the equator (Fig. 5). The east–west asymmetry in the precipitation pattern observed in experiment A4 is also seen in these experiments; the amount of precipitation decreases in the western region while it increases in the broad eastern region. As the warm SST anomaly increases, the amount of precipitation at the convection center increases (Table 2). However, the increase of precipitation in the eastern region seems to be independent of the magnitude of the SST anomaly. Even a small SST anomaly of experiment A2 causes a precipitation increase of the same magnitude as that of experiment A4. On the other hand, the drying in the western region is intensified as the warm SST anomaly increases. The western region of experiment A2 is not so dry as that of experiment A4. The drying in experiments

1 We note here that Numaguti and Hayashi (1991a, b) and Numaguti (1993) adopt different numerical codes and SST distributions. The numerical code utilized in this study, AGCM5 of GFD-DENNOU CLUB, is almost the same as that of Numaguti (1993). The basic SST distribution of this study is also the same as that of Numaguti (1993). The numerical code used by Numaguti and Hayashi (1991a, b) is based on the global spectral model of Numerical Prediction Division in Japan Meteorological Agency in the late 1980's. The SST distribution utilized in Numaguti and Hayashi (1991a, b) is obtained from the observed global SST distribution by averaging it zonally and extracting the equatorially symmetric part. The numerical code used by Numaguti (1993) was constructed by Dr. Numaguti himself on the basis of the experience of Numaguti and Hayashi (1991a, b). Those numerical codes are different significantly. The physical processes, especially, the radiative processes are completely rewritten. Numaguti (1993) also employs a simple expression of the SST distribution which roughly represents the global SST observations.

Table 2. The averaged value of precipitation and evaporation in several regions for each experiment. $\overline{P}_w$ is precipitation averaged over the warm SST area. $\overline{P}_{30}$ and $\overline{E}_{30}$ are precipitation and evaporation averaged in the tropics (between ± 30° latitudes). $\overline{P}_4$ and $\overline{E}_4$ are precipitation and evaporation averaged near the equator (between ±4° latitudes). $\overline{P}$ and $\overline{E}$ are the global averages of precipitation and evaporation. Unit is W/m^2.

Experiments	$\overline{P}_w$	$\overline{P}_{30}$	$\overline{E}_{30}$	$\overline{P}_4$	$\overline{E}_4$	$\overline{P}$	$\overline{E}$
A0	141.8	89.4	103.9	188.0	77.8	74.9	74.9
A2	197.7	89.7	104.4	197.8	78.8	75.1	75.1
A4	250.4	89.9	104.9	208.2	81.3	75.3	75.3
A6	294.5	89.1	104.6	206.0	82.8	75.0	75.0
A8	327.2	88.9	104.4	202.0	85.0	74.7	74.7
K0	108.1	84.2	94.1	85.9	72.6	70.5	70.5
K2	176.1	85.4	95.5	91.6	74.1	71.2	71.2
K4	289.2	87.9	99.1	104.9	76.5	73.1	73.1
K6	351.5	88.8	100.3	112.8	80.1	73.8	73.8
K8	335.1	88.7	100.9	132.6	79.7	73.7	73.7

A6 and A8 is intensified compared to that of experiment A4. Note that in experiments A6 and A8 the decrease of precipitation occurs even in the eastern vicinity of the warm SST area.

Figure 6 shows the temporal evolution of precipitation at the equator of experiment A4. The warm area is introduced at $t = 0$ in the figure, at which the model state is the same as that of $t = 0$ in Fig. 3 of experiment A0. By comparing Fig. 6 with Fig. 3, it is found that the western dry region is established clearly in about 20 days.

The increase of precipitation just to the north and south of the warm SST area seen in Fig. 4b is caused by intermittently generated disturbances, which are recognized as tropical depressions, propagating northward and southward from the convection center (not shown here). Contrary to this, precipitation increase in the eastern region seen in Fig. 4b is not directly caused by the generation of eastward propagating disturbances. The enhanced radiation of eastward propagating disturbances from the warm SST area does not seem to occur.

4. Structure of the east–west asymmetry in precipitation

If we could adopt the simple dynamic view mentioned in Section 1, dry regions should develop both to the east and to the west of the warm SST area, since the warming caused by waves around the active convection center should increase the static stability and hence decrease precipitation. As shown in Section 3, in the western region we have a response consistent with this expectation; a dry region appears.

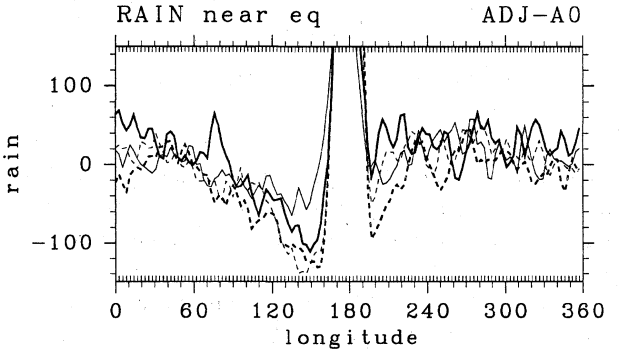

Fig. 5. Longitudinal distributions of precipitation at the equator in the warm SST area experiments. Thin solid line, thick solid line, thin dashed line and thick dashed line indicate experiments A2, A4, A6 and A8, respectively. The zonal mean precipitation value of experiment A0 is subtracted. Unit is W/m^2.

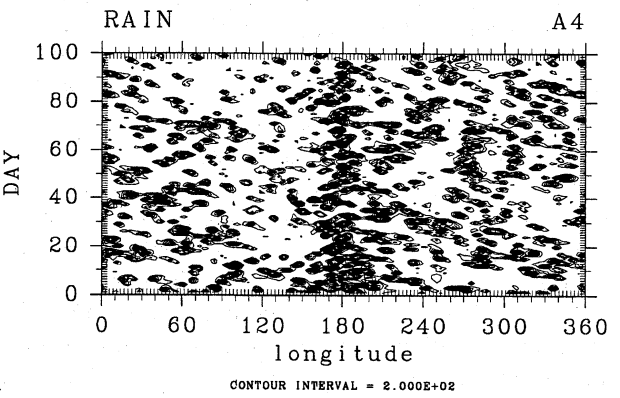

Fig. 6. Temporal evolution of precipitation at the equator of experiment A4. Contour interval is 200 W/m^2. The warm area is introduced at $t = 0$, at which the model state is the same as that of $t = 0$ in Fig. 3.

However, in the eastern region we have the opposite response to that; an increase of precipitation. In this section, in order to investigate this equatorial east–west asymmetry appearing in the precipitation response, we will consider the thermal and moisture budget as mentioned in Section 1.

4.1 Static stability

First, we examine the change of static stability induced by the warm SST area. Fig. 7a shows the difference in saturated equivalent potential temperature (θ_e^*) at the equator between experiments A4 and A0, and Fig. 7b shows that of equivalent potential temperature (θ_e). A necessary condition for occurrence of moist convection is that the value of θ_e in the lower level atmosphere is higher than the minimum of θ_e^* (usually located in the middle tro-

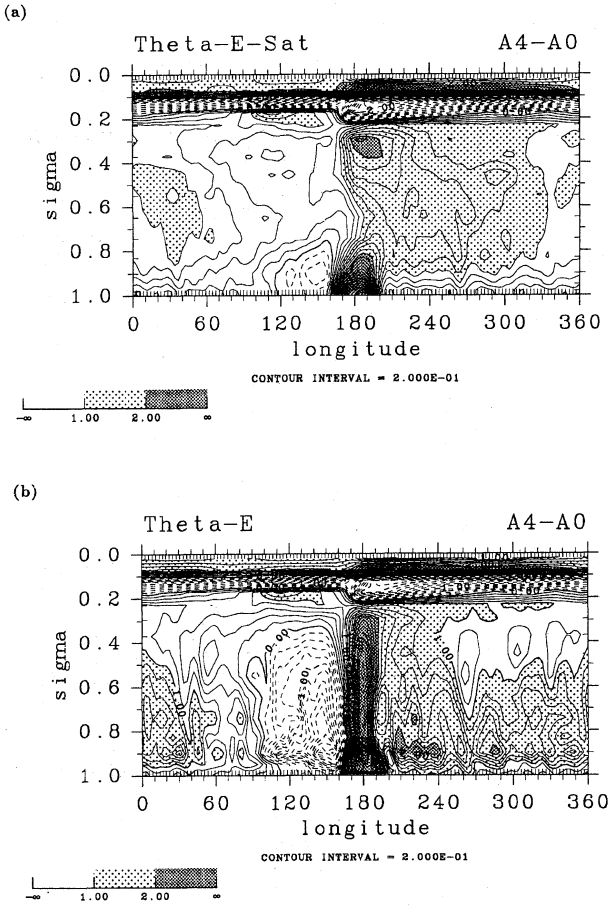

Fig. 7. (a) Equatorial longitude-height cross section of saturated equivalent potential temperature (θ_e^*) of experiment A4. (b) Same as (a) except for equivalent potential temperature (θ_e). Unit is K. The zonal mean values of experiment A0 are subtracted, respectively.

posphere).

As shown in Fig. 7a, θ_e^* increases in the middle troposphere ($\sigma \sim 0.55$) both to the east and to the west of the warm SST area. The maximum amplitude of warming is about 0.4K in the western region and about 1.5K in the eastern region. Since the increase of θ_e^* reflects the warming in the middle troposphere, its overall increase is qualitatively consistent with the previous intuitive view in which the atmosphere around a convection center is stabilized by the middle tropospheric warming. However, the fact that the eastern region is more stable (warmer) than the western region implies that precipitation should be more strongly suppressed to the east than to the west. This implication is not consistent with the response obtained in the experiments shown in Section 3.

On the other hand, in Fig. 7b, a significant east–west asymmetry can be seen in the change of θ_e in

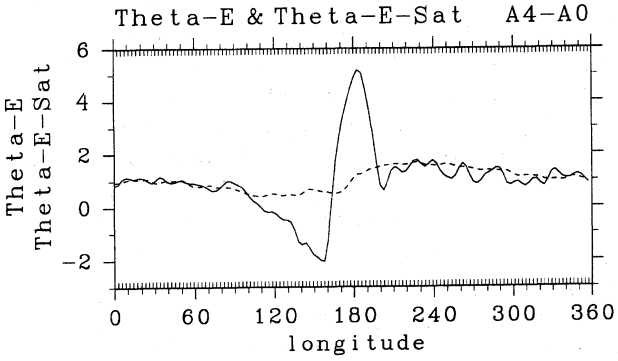

Fig. 8. θ_e at $\sigma = 0.95$ (solid line) and θ_e^* at $\sigma = 0.55$ (dashed line) along the equator. Unit is K. The zonal mean values of experiment A0 are subtracted, respectively.

the lower levels. The amplitude of its anomaly has the maximum at $\sigma = 0.9$, where its values are -2K to the west and $+2.2$K to the east. This zonally asymmetric response is consistent with that of precipitation.

Close examination of the vertical distributions of θ_e^* and θ_e reveals that the minimum of θ_e^* exists at $\sigma \sim 0.55$, and the minimum value is lower than θ_e at $\sigma \sim 0.95$ (not shown here). This implies that, in the macroscopic view represented by the moist convective adjustment scheme, the starting level of the moist convection is $\sigma \sim 0.95$. Consequently, we can diagnose the change of moist stability induced by the warm SST area by inspecting the change of θ_e at $\sigma = 0.95$ and that of θ_e^* at $\sigma = 0.55$ (Fig. 8). As evidently shown there, the stability to the east of the SST anomaly does not change appreciably, while the stability to the west increases notably; the factor most contributing to the asymmetric change of stability is the zonal asymmetry of the low level θ_e change.

4.2 Moisture budget

We will next examine the change of the moisture budget. The increase of low level θ_e to the east of the warm SST area mentioned above consists mainly of the increase of humidity; the increase of θ_e due to the temperature change is about 0.2K while that due to the moisture change is about 1K. The increase of the low level humidity to the east of the warm SST area should be accounted for either by the increase of evaporation from the ocean or by that of horizontal moisture convergence.

The importance of the surface evaporation in the tropical circulation has been emphasized in this decade. The fundamental concept is referred to as WISHE (Wind-Induced Surface Heat Exchange; Yano and Emanuel, 1991). The feedback mechanism of WISHE can be stated as follows; the large-

scale low level wind forced by cumulus convection induces the change in surface evaporation, and hence changes the moist static energy in the mixed layer, which feeds back to the activity of cumulus convection. WISHE is expected to operate in the configuration considered in this paper, because the anomalous easterly to the east of the warm SST area can increase evaporation there since the basic zonal wind is easterly in the reference state with the zonally uniform SST distribution.

The importance of moisture convergence, on the other hand, is most notably mentioned in the CISK theory associated with frictional convergence in the boundary layer. The feedback mechanism of CISK can be stated as follows; the heating generated by cumulus convection induces the large-scale response of pressure distribution, and succeedingly the change of low level frictional flow, which modifies the distribution of moisture convergence. This intensifies the activity of cumulus convection. CISK is also expected to operate in the present configuration because the Kelvin wave-like response is expected to produce low pressure area to the east of the convection center at the equator, which should be accompanied by the convergence of low level frictional flow. This convergence may modify the cumulus distributions in the distant region from the warm SST area.

In the following paragraphs, we will evaluate the relative importance of the two candidates, WISHE and CISK, by examining the response of evaporation and that of the difference between precipitation and evaporation (indicated by $P-E$ below) which reflects the horizontal moisture convergence.

Figure 9a shows the difference in evaporation in the tropics between experiments A4 and A0, and Fig. 9b is that for $P-E$. Around $\pm 7°$ latitudes to the east of the warm SST area, a slight increase of evaporation is found. However, against the previous expectation on WISHE, the equatorial response to the east of the warm SST area is negative. On the other hand, $P-E$ increases at the equator to the east of the warm SST area. As $P-E$ equals a horizontal moisture convergence in the equilibrium state, this indicate the existence of significant horizontal moisture convergence at the equator to the east of the warm SST area. It is evident that the change of evaporation does not play an important role in moistening at the equator.

In order to show the responses more clearly, the changes of evaporation and precipitation at the equator are plotted in Fig. 10a. Again, it is evident that precipitation is enhanced to the east of the warm SST area and suppressed to the west. The change in evaporation, on the other hand, is very small compared to that of precipitation except for over the warm SST area.

Figure 10b shows the longitudinal distributions

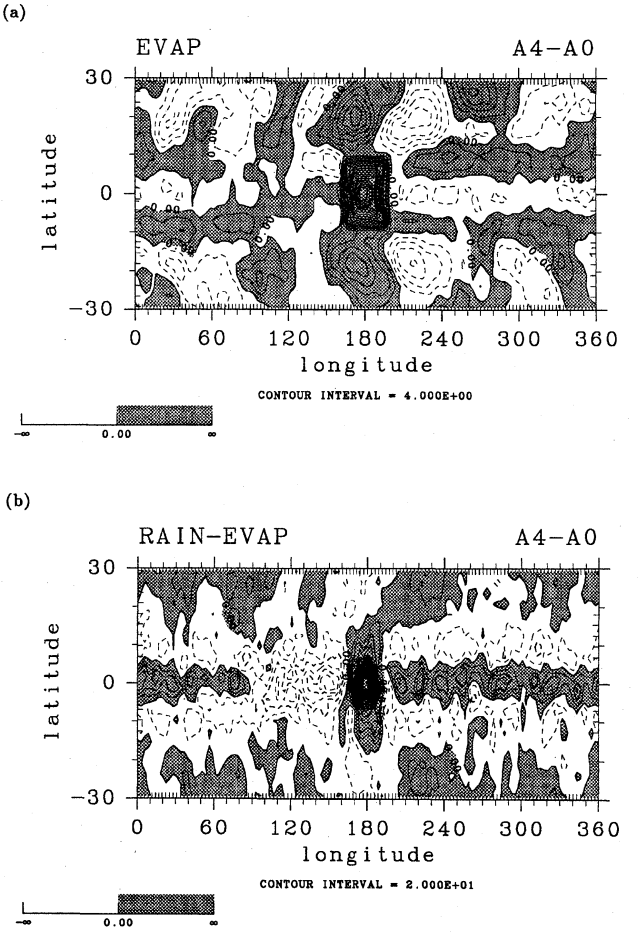

Fig. 9. Horizontal distributions of (a) evaporation and (b) $P-E$ of experiment A4. Unit is W/m^2. The zonal mean values of experiment A0 are subtracted, respectively.

of the changes of precipitation and evaporation averaged meridionally between $\pm 30°$ latitudes. There is no east–west asymmetry in the evaporation response, just as at the equator. WISHE does not operate even as the meridional average over the whole tropical latitudes.

By comparing Fig. 10a and Fig. 10b, we recognize that the increase of precipitation in the eastern region at the equator (Fig. 10a) is compensated by the decrease of that in the subtropics, resulting in little change in the meridionally averaged precipitation (Fig. 10b). This suggests that the equatorial precipitation enhancement to the east of the warm SST area is accounted for by the change of meridional moisture transport.

The enhancement of precipitation at the equator by the change of the meridional moisture flux to the east of the warm SST area can be recognized also in the other experiments with different amplitudes of the warm SST anomaly. The increases of precipitation at the equator in the eastern region are evident

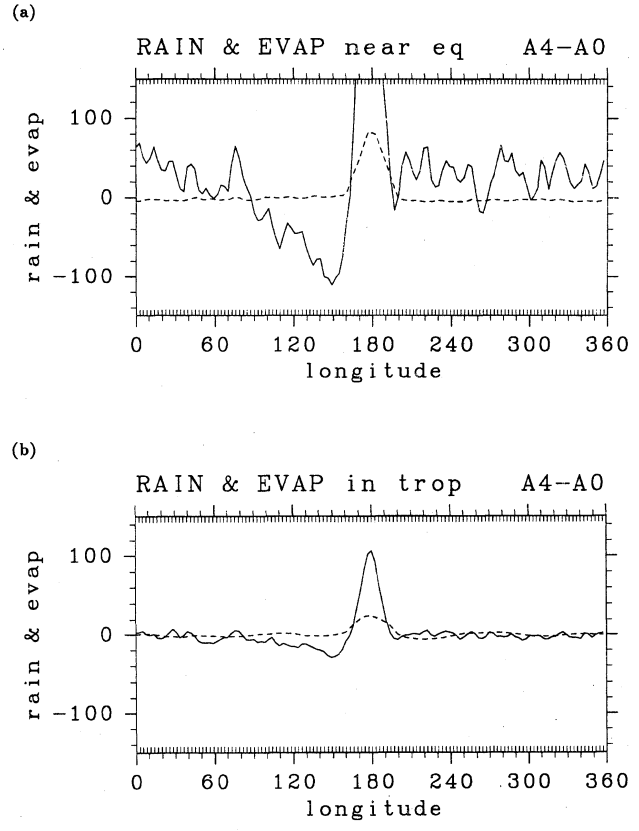

Fig. 10. Longitudinal distributions of precipitation (solid line) and evaporation (dashed line) of experiment A4 (a) at the equator and (b) averaged in the meridional area between ±30° latitudes. Unit is W/m^2. The zonal mean values of experiment A0 are subtracted, respectively.

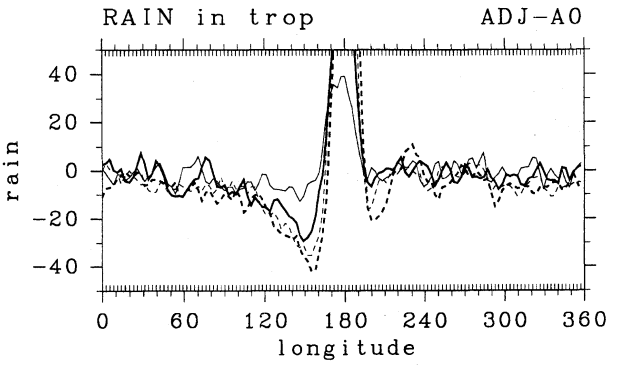

Fig. 11. Longitudinal distributions of precipitation averaged meridionally in the tropical region between ±30° of the warm SST experminets. Thin solid line, thick solid line, thin dashed line and thick dashed line indicate experiments A2, A4, A6 and A8, respectively. The zonal mean precipitation value of experiment A0 is subtracted. Unit is W/m^2.

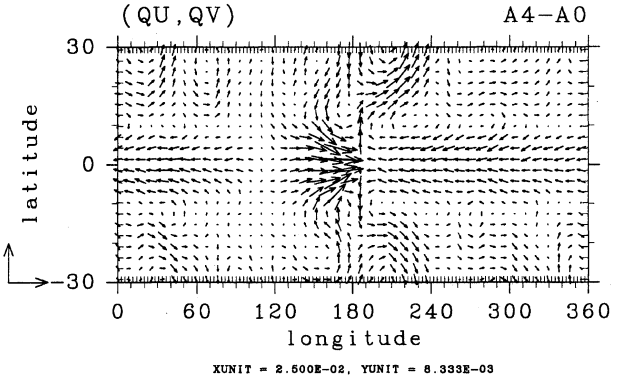

Fig. 12. Horizontal distribution of the temporal mean and vertically integrated moisture flux (qu, qv) of experiment A4. Zonal average moisture flux of experiment A0 is subtracted.

in all experiments (Fig. 5), but meridionally averaged responses are nearly equal to zero (Fig. 11) as in experiment A4 described previously.

The difference of the vertically integrated moisture flux of experiment A4 from A0 is shown in Fig. 12. On top of the large vectors directed zonally along the equator converging to the warm SST area, there exist moisture flux vectors directed meridionally around 10° latitudes converging into the equatorial enhanced precipitation zone to the east of the warm SST area.

Moisture transports in the zonal and meridional directions shown in Fig. 12 are different in their vertical profiles (not shown). The moisture transport in the zonal direction along the equator extends vertically up to about 700 hPa level, while the moisture transport in the meridional direction around 10° latitudes is confined below 900 hPa. This is the level under which the effect of surface friction is significant in the model.

Figure 13 summarizes the difference of large-scale circulations between experiments A4 and A0. As evident in Fig. 13c, the surface pressure anomaly is negative in wide area to the east of the warm SST area and is most significant at the equator. Corresponding to this pressure anomaly, horizontal wind converging toward the equator is notable in the region of large anomalous pressure gradient at around the latitudes of $\pm 5° \sim 8°$. This is an evidence that the converging flow occurs as a surface frictional flow. The moisture transport anomaly in the meridional direction is realized by this frictional flow.

At the same time Fig. 13c shows that the region of enhanced surface easterly is quite limited in a narrow region near the warm SST area. This is a reason for the absence of WISHE in producing the east–west asymmetry of the precipitation pattern.

Figure 13b shows the equatorial cross section of the anomalies of circulation and temperature of ex-

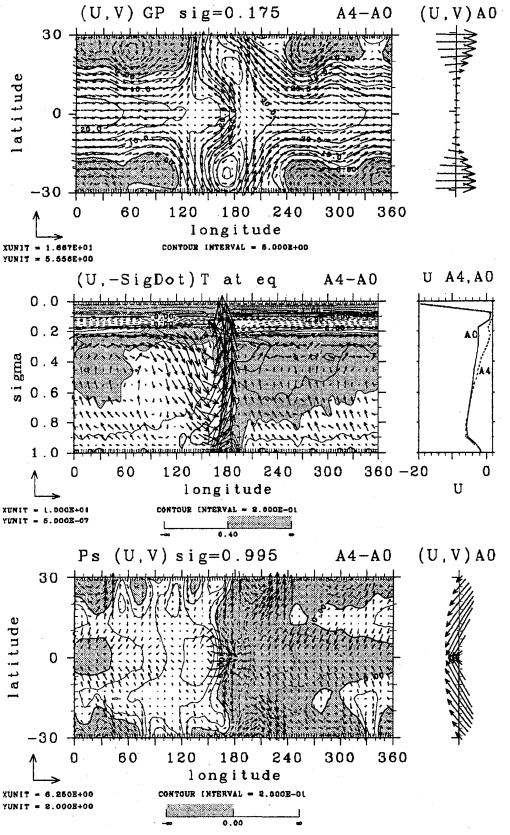

Fig. 13. Changes in the tropical circulation in experiment A4 from the zonal means of experiment A0; (a) horizontal distributions of wind vector and geopotential height at $\sigma = 0.175$, (b) vertical cross section of temperature and circulation (u and σ velocity) at the equator, (c) horizontal distributions of wind vector at the lowest level ($\sigma = 0.995$) and surface pressure. The panels in the right hand side of each figure indicate (a) zonally averaged wind vector in experiment A0 at $\sigma = 0.175$, (b) vertical cross section of zonally averaged zonal wind at the equator in experiment A0 and A4, (c) zonally averaged wind vector in experiment A0 at $\sigma = 0.995$.

periment A4 from those of experiment A0. The longitudinal distribution of vertical velocity is well correlated with that of precipitation (Fig. 10a). Especially to the west of the warm SST area, there exists a region of strong downward motion whose zonal extent is almost the same as that of the negative precipitation anomaly. The coexistence of the downward motion and drying to the west of the warm SST area appears in all of the warm SST anomaly experiments (A2 $\sim$ A8).

In Fig. 13b, a region of the positive temperature anomaly is spreading widely to the east of the warm SST area. This corresponds to the extension of negative surface pressure anomaly in the eastern area of Fig. 13c. Furthermore, the direction of the wind vectors in the lower and upper troposphere in the equatorial region are westward and eastward respectively (not shown); there are little meridional components except for those in the lowest layers. These are the features of Kelvin waves and hence the circulation in the widely spreading eastern region can be regarded as an equatorial Kelvin wave-like response.

Figure 13a shows the changes of horizontal wind and geopotential height at the upper troposphere ($\sigma = 0.175$). It is evident that the zonal mean wind anomaly at this level is westerly. Correspondingly, ejection of Rossby wave-like trains to the mid-latitudes is observed. The wave trains are more clearly seen in the global geopotential height field (not shown here). The Rossby wave-like trains are anticipated to carry easterly momentum to the extratropics. The detailed examination in this aspect will be presented elsewhere.

4.3 Experiments without WISHE

As a result of moisture budget analyses presented in the previous subsection, we may conclude that it is not WISHE but frictional convergence that contributes to the generation of the east–west asymmetry in the equatorial precipitation response. In order to evaluate the effect of WISHE more completely, experiment A4VC is conducted in which WISHE is excluded artificially.

In the numerical model utilized in this paper, evaporation from the sea surface is calculated by the use of the bulk formula. In experiment A4VC, the surface wind speed used in this evaporation formula is held constant in time in the tropical region between the latitudes of $\pm$ 30°. The fixed value of constant wind speed is obtained from the temporal and zonal mean of experiment A0 except for the warm SST area where the temporal mean value of experiment A4 is used. The initial condition of experiment A4VC is the data at day 2200 of experiment A0 and is integrated for 900 days and the data of the last 500 days is used for the following analyses (Fig. 14, Fig. 15).

As is evident in Fig. 14a, precipitation at the equator to the east of the warm SST area increases significantly from that of experiment A0. The response in $P - E$ (Fig. 14b) is quite similar to that of experiment A4 (Fig. 9b). This shows that the precipitation response is strongly connected to the horizontal moisture convergence. The longitudinal distributions of precipitation and evaporation at the equator and their averages in the tropical region (Figs. 15a,b) are also similar to those of experiment A4 (Figs. 10a,b). These results clearly show that WISHE plays at most secondary role in the generation of the zonally asymmetric response of precipitation.

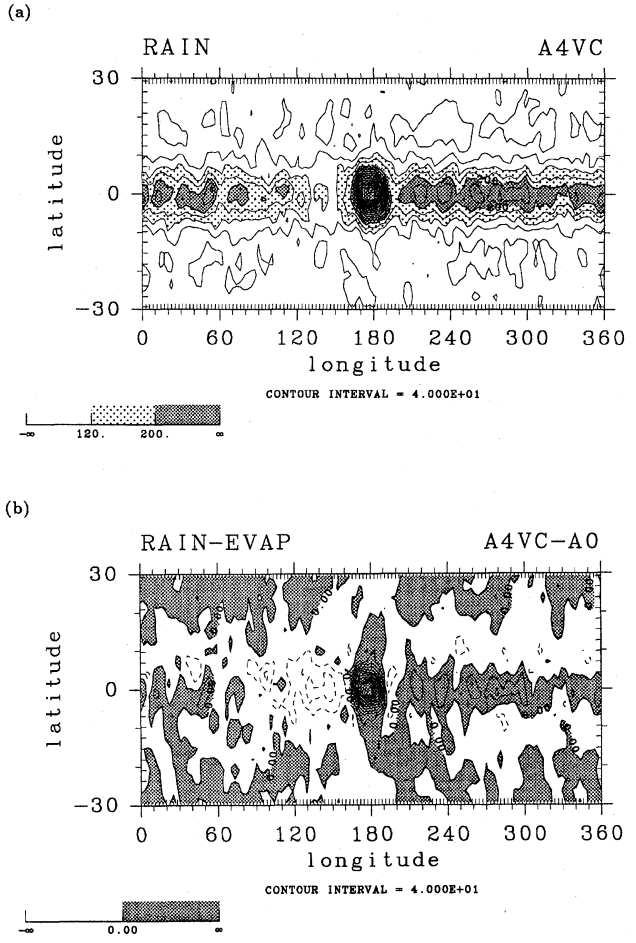

Fig. 14. Horizontal distributions of the resuluts of experiment A4VC; (a) precipitation and (b) $P - E$ anomaly from the zonal mean value of experiment A0. Unit is W/m^2.

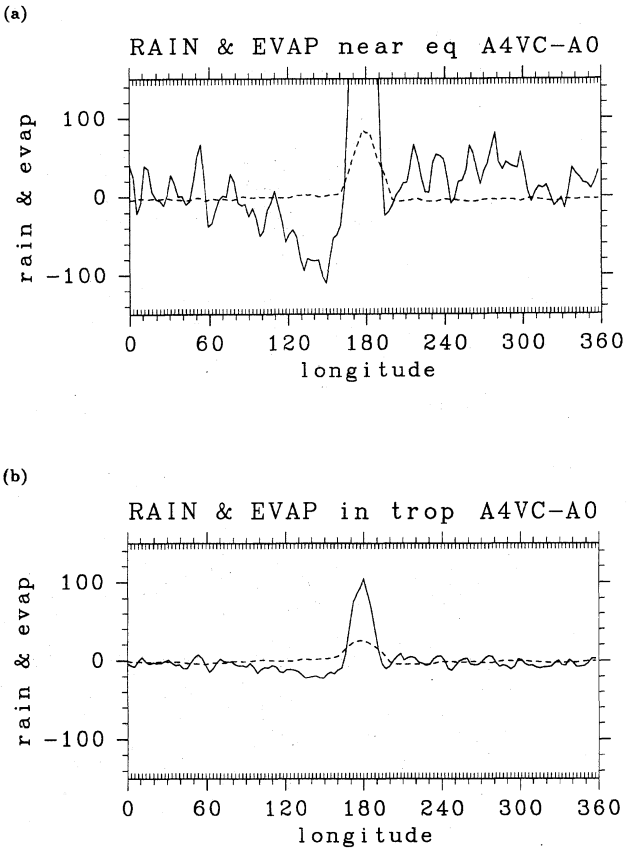

Fig. 15. Longitudinal distributions of precipitation (solid line) and evaporation (dashed line) of experiment A4VC (a) at the equator and (b) averaged in the meridional area between ±30° latitudes. Unit is W/m^2. The zonal mean values of the experiment A0 are subtracted, respectively.

5. Experiments with the Kuo scheme

In this section, we will present the results of experiments with the Kuo scheme instead of the adjustment scheme to examine the sensitivity of the precipitation structure to the choice of the cumulus parameterization scheme.

Firstly, we briefly present the results of the experiment without the warm SST area (experiment K0). As shown in Fig. 16, the distribution of the zonally averaged precipitation has two peaks in the tropics at the latitudes of ±7° and a minimum at the equator. This is the well-known feature of the sensitivity of ITCZ to the choice of the cumulus parameterization (Numaguti, 1993; Hess *et al.*, 1993).

Figure 17a shows the horizontal distribution of precipitation in experiment K4, and Fig. 17b shows its difference from the zonal mean distribution of experiment K0. Although the positions of ITCZs of experiment K0 are significantly different from that of experiment A0, the precipitation response charac-

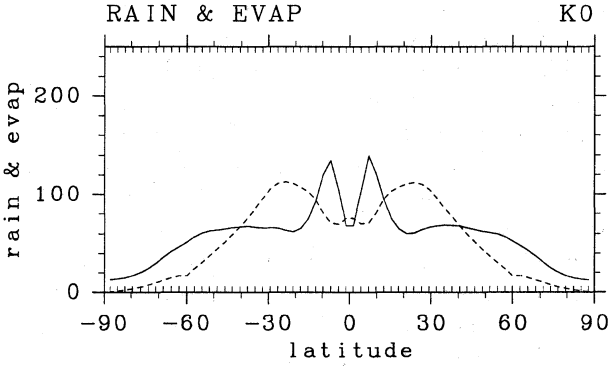

Fig. 16. Latitudinal distributions of temporal and zonal mean precipitation (solid line) and evaporation (dashed line) of experiment K0. Unit is W/m^2.

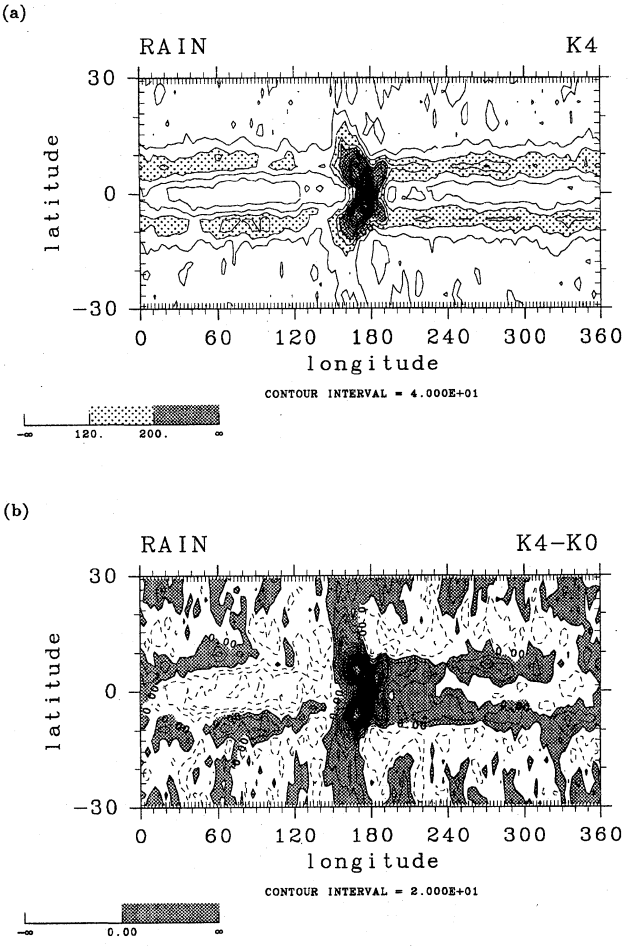

Fig. 17. (a) Time mean horizontal distribution of precipitation for experiment K4. (b) Its difference from the zonal mean distribution of experiment K0. Unit is W/m^2. Contour intervals are (a) 40 W/m^2 and (b) 20 W/m^2.

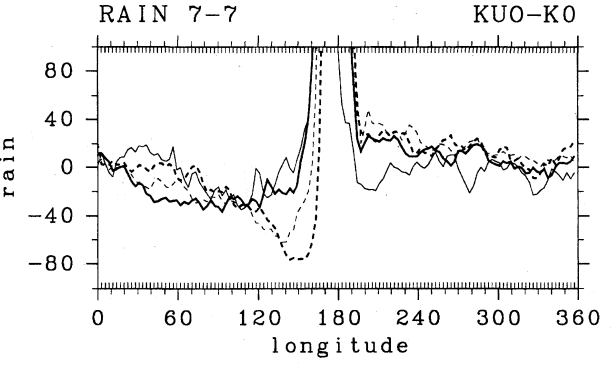

Fig. 18. Longitudinal distributions of precipitation averaged over the latitudinal region between ±7 degrees for the warm SST area experiments of the K series. Thin solid line, thick solid line, thin dashed line and thick dashed line indicate experiments K2, K4, K6 and K8, respectively. The zonal mean precipitation value of experiment K0 is subtracted. Unit is W/m^2.

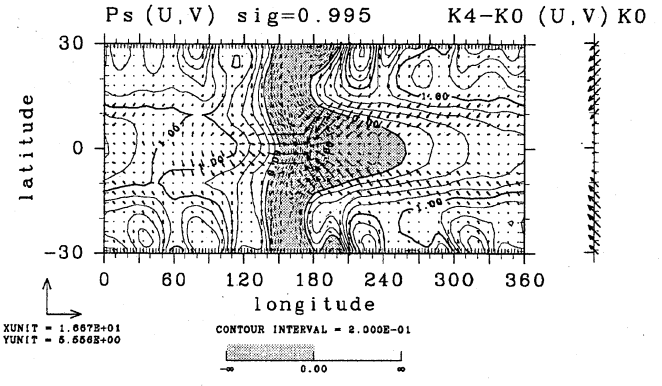

Fig. 19. Changes of horizontal distributions of wind vector at the lowest level (σ = 0.995) and surface pressure in experiment K4 from the zonal means of experiment K0. The panel in the right hand side indicates zonally averaged wind vector in experiment K0 at the same σ level.

terized by the appearance of the east–west asymmetry is qualitatively similar; precipitation increases to the east of the warm SST area while a dry region appears to the west. This tendency is clearly seen in Fig. 18, which shows the longitudinal distributions of precipitation averaged over the latitudinal region between ±7 degrees. As the peak value of SST anomaly is increased, the east–west asymmetry becomes evident and tends to have the characteristics similar to that of A-series experiments.

Figure 19 shows the differences of wind vector at the lowest level (σ = 0.995) and surface pressure between experiments K4 and K0. The characteristics observed in experiment A4 (Fig. 13c) also appear in Fig. 19. The surface pressure anomaly is negative to the east of the warm SST area, while it is positive to the west. In the eastern side, the negative pressure anomaly is most significant at the equator, and correspondingly, the horizontal wind converging toward the equator is notable in the region of large anomalous pressure gradient. At the same time, the positive temperature anomaly exists above the equatorial low pressure area and correspondingly, zonally-directed wind exists above the surface boundary layer (not shown). These are the features of Kelvin waves and hence the circulation in the eastern region can be regarded as an equatorial Kelvin wave-like response.

Figure 19 also shows that the region of enhanced surface easterly is quite limited in a narrow region near the warm SST area. The narrowness of the enhanced surface wind region has been also observed in Fig. 13c of the experiment A4. This suggests that

WISHE does not operate in producing the east–west asymmetry of the precipitation pattern. In order to confirm this expectation, we conducted experiment K4VC in which WISHE is artificially suppressed just as experiment A4VC. The results (not shown here) are quite similar to that of experiment K4.

Those similarities of the responses between experiments K series and A series proves that the main reason for the appearance of the east–west asymmetry in the precipitation response is not WISHE but horizontal moisture convergence. The structure is robust in the sense that it does not depend on the cumulus parameterization scheme utilized.

6. Conclusions and discussions

6.1 Conclusions

By a series of aqua planet experiments with a localized warm SST area with various intensities, the following conclusions are obtained. The response to a warm SST area placed at the equator is that precipitation is enhanced in an extensive region to the east of the warm SST area while drying occurs to the west. The increase of precipitation in the eastern region results from the increase of meridional moisture convergence associated with the frictional inflow converging into the low pressure area existing to the east of the warm SST area. The decrease of precipitation in the western region is associated with downward flow and an increase of stability due to a temperature rise in the middle layer. WISHE does not play an important role in the generation of the east–west asymmetry of the precipitation response.

By comparing the results of the two series of experiments with the different cumulus parameterization schemes (the adjustment scheme and the Kuo scheme), the structure of the precipitation response is found to be insensitive to the choice of cumulus parameterization scheme. The east–west asymmetric response of precipitation obtained in the present study is robust in this sense.

The characteristic that an intense dry region appears to the west of an active convection center is found in the real tropical atmosphere and the GCM experiments. During the ENSO warm events, strong droughts are observed to the west of the warm SST anomaly areas in the equatorial Pacific (Ropelewski and Halpert 1987). In the 82–83 ENSO warm event, the decrease of cumulus activity is clearly shown by the OLR observation (*e.g.*, Arkin *et al.* 1983); it is reported that forest fires occurred even in the tropical rain forest of Borneo (Tsuyuki, 1988) In the GCM SST anomaly experiments, dry areas also appear to the west of the anomalous regions (*e.g.*, Keshavamurty, 1982; Geisler *et al.*, 1985; Wu and Liu, 1992). As for the climatic precipitation distribution, there appear small rainfall regions to the west of the convection centers (Spencer, 1993). For instance, the heavy convection activity over the Maritime Continent does not extend westward far into the Indian Ocean along the equator. The reason for the small rainfall is usually considered a result of low SST values in the corresponding region. However, even if the values of SST to the eastern and western sides are the same, the results of present research show that a dry region extends to the west of the convection center. The characteristics exemplified in our numerical calculations contribute at least partly to the formation of precipitation patterns to the west of the real convection centers.

From the theoretical framework presented in the literature in the past, our numerical results raise at least the following two issues. The first is to consider to what extent the tropical thermal response theory demonstrated by Gill (1980) and others is applicable to describe our numerical results. The appearance of dry region to the west of the warm area has not been expected to appear as simple long wave response to a localized heating, and will be one of the key issues to be investigated. The second is to consider in what situation WISHE can be a dominant contributer for precipitation patterns. In the preceding studies (Numaguti and Hayashi, 1991b; Numaguti, 1993), WISHE has been revealed as an important mechanism to produce and/or maintain large scale precipitation patterns (MJO and ITCZs), while in this study WISHE has at most secondary effects. In the following subsections, we will try to describe the structure of dry and wet area by the equatorial long-wave dynamics, and also we will try to discuss the reason for WISHE being inefficient. We have to confess beforehand that the arguments to be presented hereafter remain within the scope of speculation. However, we believe that a qualitative discussion should be placed from the bases of our experimental results and the knowledge of the previous works on forced response problems with the equatorial wave dynamics.

6.2 Dry area, secondary negative heat source, and wave dynamics

In a usual simple argument about the effect of a warm SST area on a circulation field, only a single local heat source representing the precipitation increase over the warm SST area has been assumed. However, in our results, the precipitation difference outside of the warm SST area should also be regarded as heating and/or cooling which contributes modification of the circulation field. In order to compare the amount of this "secondary" heat source outside of the warm SST area to that of the "primary" heat source over the warm SST area, Table 3 lists the differences of the amounts of precipitation integrated over various key areas for ex-

2 The forest fires of 97 event are recently reported to be even more severe.

Table 3. The differences of precipitation A4 from A0 and K4 from K0 integrated over the following areas (Unit is W). For experiment A4, "Western area" indicates the area between the longitudes 90° and 160°, "Convection Center" indicates the area between the longitudes 160° and 191°, "Eastern area" indicates the remaining longitudinal area. For experiment K4, they indicate between the longitudes 10° and 150°, between the longitudes 150° and 197°, and the remaining longitudinal area, respectively. The latitudinal extent of those areas is from −10° to +10°. The remaining zonally integrated subtropical precipitation differences are also listed for the latitudes from +30° to +10° and −10° to −30°

Experiments	Lat	Western area	Convection Center	Eastern area
A4-A0	+30∼+10	-1.16×10^{14}		
	+10∼−10	-7.31×10^{14}	1.21×10^{15}	-0.96×10^{13}
	−10∼−30	-2.12×10^{14}		
K4-K0	+30∼+10	-3.97×10^{14}		
	+10∼−10	-6.07×10^{14}	2.16×10^{15}	2.65×10^{14}
	−10∼−30	-4.64×10^{14}		

periments A4 and K4. Table 3 indicates that the secondary heat sources cannot be neglected compared to the primary heat sources. The noteworthy point is that, especially in experiment A4, the total amount of the decrease of precipitation in the western area (-7.31×10^{14} W) exceeds half of the increase of total precipitation over the warm SST area (1.21×10^{15} W). In order to understand the circulation fields caused by the existence of the warm SST area, the secondary negative heat source caused by the precipitation decrease should also be considered.

There are two issues to be considered with the secondary heat source. The first is the problem of maintenance. As will be mentioned below, we are speculating that the gross characteristics of the circulation fields can be understood within the framework of equatorial wave theory (*e.g.*, Gill 1980 and others) by considering the existence of the secondary heat source. The second is the problem of causality. In this paper, we have not completed the description of the formation of secondary heat source distribution (precipitation change). This issue will be briefly mentioned in the next subsection.

Corresponding to the existence of the secondary negative heat source, the important characteristic to be marked is the existence of the high pressure anomaly area to the west of the warm SST area. As is evident from Fig. 13c and Fig. 19, there exist high pressure anomalies to the west of the convection center. According to the equatorial linear long-wave theory, westward propagating Rossby waves generated from the primary positive heat source (convection center) should create a surface low pressure anomaly just as do eastward propagating Kelvin waves (Gill 1980). The western high surface pressure anomalies of our experimental results cannot be expected from a linear long-wave response to a single heat source. However, we can recognize the existence of those high pressure anomalies as the effect of the secondary negative heat source. Since, as mentioned above, the amount of the negative heat source is fairly large, the low pressure anomaly from the convection center may be overwhelmed by the high pressure anomaly created by the negative heat source caused by the precipitation decrease. If this is the case to our numerical results, we do not have to change the framework of Gill, (1980) but cather include the secondary negative heat source instead of the single heat source over the warm SST area to crudely understand the structure of the circulation field.

The similar pressure responses can be observed along the off-equatorial tropical latitudes. The surface low pressure anomalies around 10 ∼ 20° latitudes end just in the western neighborhood of the warm SST area; at around 165° for experiment A4 (Fig. 13a) and around 140 ° for experiment K4 (Fig. 19). To the west of those longitudes, the surface pressure anomalies become high. In the upper troposphere around ±20° latitudes, the anticyclonic circulations from the convection center do not extend far into the west. The cyclonic circulations appear instead at around 165° for experiment A4 (Fig. 13a) and around 140 ° for experiment K4 (not shown). Recalling that the geopotential peaks of the fundamental mode of equatorial Rossby wave appear at the latitudes of $\sqrt{3/2}$ times equatorial radius of deformation which is $\sqrt{3/2}\times$(1300–1600) km for $c = 40 - 60$ m/s, those off-equatorial tropical circulation characteristics can be regarded as a superposition of the long Rossby wave generated by the convection center and that generated by the secondary negative heating caused by the precipitation decrease to the west of the warm SST area.

Those features suggest that the gross characteristics of the circulation fields seem to be consistent with the expectation of equatorial wave response to a thermal forcing (Gill, 1980) but with recalling the existence of the secondary heat source. However, the scenario needs more quantitative verification. In experiment A4, the amount of western negative heating is only about a half of the positive heating of the convection center (Table 3). In experiment K4, it is even smaller. We are speculating that dissipation processes reduce the amplitude of emitted waves as traveling from the sources and hence, in the neighborhood of the negative heating area, the high pressure anomaly overwhelms the low pressure signal from the east.

Most of the investigations with simple models

on heating anomaly response problems presented so far consider responses to a single one-signed heating anomaly or realistic ones (Gill, 1980; Lim and Chang, 1983; Lim and Chang, 1986; Gill and Philips, 1986; Hendon, 1986). Ting and Held (1990) performs GCM experiments with dipole tropical SST anomaly, but, since they focus exclusively on the extratropical responses, they present little information on the tropics related to our problems. We have to design new experiments in order to check our speculations.

6.3 Formation of precipitation Change

So far, we have not shown how the increase and/or decrease of precipitation establishes after placing the warm SST area. What we have shown from our experimental results is that the precipitation distribution is consistent with the surface wind convergence. We have described in Section 4 and Section 5 that the frictional convergence due to Kelvin wave-like structure causes the precipitation increase to the east of the warm SST area. However, we have used the term 'Kelvin wave' only because the circulation structures and the low level winds obtained by the experiments resemble the characterisitics of equatorial Kelvin waves (Fig. 13 and Fig. 19); we have not verified that the development of the equatorial low pressure region to the east of the warm SST area is an equatorial Kelvin wave response ejected from the convection center. In the western part, we have not described the frictional divergence by the use of 'Rossby wave'. The circulation structures of this area seem to be complicated as discused in the previous subsection.

In the eastern region, it can be expected that, at the start of the warm SST area experiments, the positive temperature signal in the middle troposphere and the surface low pressure signal emitted from the convection center formed as the intrusion of the warm SST area propagate eastward with the speed of the equatorial Kelvin wave and cover the entire tropics. Motivated by this expectation, we examined time evolutions of tropospheric temperature and surface pressure at the equator just after the start of the warm SST area experiments (not shown here). Unfortunately, because of the abundant existence of the background waves generated by the natural convective activity in the tropics, the clear identification of the signals emanating from the warm SST area is difficult; the expected picture of the Kelvin wave propagation has not been confirmed. In order to obtain explicit evidence on this issue, one should perform ensemble experiments starting from different initial conditions to eliminate the background wave activities.

As for the dry and high pressure anomaly area to the west of the convection center, we present a following scenario. The switching on of the warm SST area generates the long Rossby wave response to the west associated with low pressure anomaly. The difference in the western Rossby wave response compared to the eastern Kelvin wave response is that the centers of the low pressure are located in the northern and southern hemispheres; the equatorial pressure anomaly is relatively high compared to other latitudes. The resultant surface frictional wind in the mixed layer is divergent at the equator; this wind suppress as the water vapor convergence and moist convection activity there. Consequently, the thermal forcing in this area tends to be negative and enhances the surface high pressure anomaly there. In order to check this scenario, we have to carry out ensemble experiments as previously mentioned in the argument of the eastern response, which remains an issue of further investigations.

6.4 Wind responses and WISHE

According to Numaguti and Hayashi (1991b) and Numaguti (1993), WISHE is shown to be crucially important for the maintenance of MJO and ITCZ in the aqua planet experiments. Interestingly, however, WISHE has proven to be unimportant for the generation of the east–west asymmetric precipitation pattern resulting from the warm SST area.

An interesting result which may be relevant to the inefficiency of WISHE is that the surface wind anomaly at the equator is confined to the neighborhood of the warm SST area. As seen in Fig. 13c, the amplitude of the equatorial surface wind anomaly exceeds 1 m/s only in the region between the longitudes of 150° and 200°. On the other hand, in the lower troposphere above the level of $\sigma = 0.9$, the equatorial wind anomaly to the east of the warm SST area extends uniformly to the distance. These characteristics of the wind anomaly can be seen by a close examination of Fig. 13b.

We are expecting that the strong momentum damping in the boundary layer is the probable reason for the small amplitude of surface zonal wind anomaly along the equator away from the warm SST area. A disturbance can propagate only for a small horizontal distance in the boundary layer because of the large dissipation effect. However, in the troposphere above the boundary layer, a disturbance can propagate for a long distance. The tropospheric disturbance above the boundary layer seems to have little direct influence on the surface wind because of large dissipation. The surface pressure, however, can be influenced by the tropospheric disturbance mentional previously, through the hydrostatic relationship. The resultant surface pressure disturbance causes surface wind anomaly at the places where the pressure gradient exists. The equatorial surface wind response is expected to be very small because of the small pressure gradient expected there.

The narrow extent of the surface wind response re-

minds us of the arguments on the tropical low-level wind distribution by Lindzen and Nigam (1987) and Neelin (1988, 1989). They show that the large dissipation rates should be implemented in the shallow water models to realize a realistic wind distribution for a given realistic horizontal distribution of heating (mass source) or SST gradient (momentum source). However, their systems, which are basically one layer models, can not include the remote influence through the wave propagation in the troposphere above the boundary layer. We need more quantitative discussion about the role of vertically varying dissipation on the remote influence before considering the consistency of our results with the previous arguments.

In the problems of MJO (Numaguti and Hayashi, 1991b) and ITCZ (Numaguti, 1993), where WISHE is important as a maintenance mechanism, the amplitudes of the related zonal wind anomalies are large in the wide longitudinal area. In the MJO of Numaguti and Hayashi (1991b), the surface wind anomaly associated with MJO is about 1 m/s, while the zonal mean value of the surface wind averaged in the equatorial region between $\pm 10°$ latitudes is about 3 m/s. In the ITCZ transition experiments in Numaguti (1993), the Change from double to single-ITCZ structure takes place when the wind speed in evaluating evaporation is fixed to be 6 m/s, while the wind speed is 3.5 m/s at the equator and 7.5 m/s in the subtropics under the double ITCZ condition. Compared to those experiments, the surface wind anomalies in the present warm SST area experiments are considerably small. As seen in Fig. 13c, the low level zonal wind anomaly averaged in the equatorial region between $\pm 10°$ latitudes is at most 0.5 m/s, which is by an order of magnitude smaller than the surface wind speed (about 6 m/s) of experiment A0 averaged over the same latitudes.

The surface wind anomaly observed in our experiments is small, while that of MJO in Numaguti and Hayashi (1991b) is large. At the moment, we cannot tell whether these two experiences are consistent to each other or not. We now feel that responses to steady and moving heat sources seem to have different features because of the effect of the boundary layer. Thorough understanding of these points requires properly designed, different sets of numerical experiments, which are left for future works.

Acknowledgments

The numerical integrations were performed at the supercomputer (NEC SX-3) of the Center for Global Environmental Research, National Institute for Environmental Studies. The softwares and local computation/information environments were constructed with the use of the resources of GFD-DENNOU CLUB.

References

Arkin, P.A., J.D. Kopman and R.W. Reynolds, 1983: 1982–1983 El Nino/Southern Oscillation event quick look atlas. NOAA/National Weather Service, National Meteorological Center, Climate Analysis Center, Washington D.C. 20323.

Emanuel, K.A., 1987: An air-sea interaction model of intraseasonal oscillations in the tropics. *J. Atmos. Sci.*, **44**, 2324–2340.

GFD-DENNOU CLUB, 1997: AGCM5/GFD-DENNOUCLUB version (in Japanese). URL: http://dennou-k.gaia.h.kyoto-u.ac.jp/.

Geisler, J.E., M.L. Blackmon, G.T. Bates and S. Munoz, 1985: Sensitivity of January climate response to the magnitude and position of equatorial Pacific sea surface temperature anomalies. *J. Atmos. Sci.*, **42**, 1037–1049.

Gill, A.E., 1980: Some simple solutions for heat-induced tropical circulation. *Quart. J. Roy. Metor. Soc.*, **106**, 447–462.

Gill, A.E. and P.J. Phlips, 1986: Nonlinear effects on heat-induced circulation of the tropical atmosphere. *Quart. J. Roy. Meteorol. Soc.*, **112**, 69–91.

Hayashi, Y.-Y. and A. Sumi, 1986: The 30-40 day oscillations simulated in an "aqua planet" model. *J. Meteor. Soc. Japan*, **64**, 451–467.

Hendon, H.H., 1986: The time-mean flow and variability in a nonlinear model of the atmosphere with tropical diabatic forcing. *J. Atmos. Sci.*, **43**, 72–88.

Hess, P.G., D.S. Battisti and P.J. Rasch, 1993: Maintenance of the intertropical convergence zones and the large-scale tropical circulation on a water-covered Earth *J. Atmos. Sci.*, **50**, 691–713.

Keshavamurty, R.N., 1982: Response of the atmosphere to sea surface temperature anomalies over the equatorial Pacific and the teleconnections of the southern oscillation. *J. Atmos. Sci.*, **39**, 1241–1259.

Kuo, H.L, 1974: Further studies of the parameterization of the influence of cumulus convection on large-scale flow. *J. Atmos. Sci.*, **31**, 1232–1240.

Lim, H. and C.-P. Chang, 1983: Dynamics of teleconnections and Walker circulations forced by equatorial heating. *J. Atmos. Sci.*, **40**, 1897–915.

Lim, H. and C.-P. Chang, 1986: Generation of internal- and external-mode motions from internal heating: effects of vertical shear and damping. *J. Atmos. Sci.*, **43**, 948–57.

Lindzen, R.S. and S. Nigam, 1987: On the role of sea surface temperature gradients in forcing low level winds and convergence in the tropics. *J. Atmos. Sci.*, **44**, 2418–2436.

Manabe, S., J. Smagorinsky and R.F. Strickler, 1965: Simulated climatology of a general circulation model with a hydrologic cycle. *Mon. Wea. Rev.*, **93**, 769–798.

Mellor, G.L. and T. Yamada, 1974: A hierarchy of turbulence closure models for the planetary boundary layers. *J. Atmos. Sci.*, **31**, 1791–1806.

Neelin, J.D., 1988: A simple model for surface stress and low-level flow in the tropical atmosphere driven by prescribed heating. *Quart. J. Roy. Meteorol. Soc.*, **114**, 747–770.

Neelin, J.D., 1989: On the interpretation of the Gill model. *J. Atmos. Sci.*, **46**, 2466–2468.

Neelin, J.D., I.M. Held and K.H. Cook, 1987: Evaporations-wind feedback and low-frequency variability in the tropical atmosphere. *J. Atmos. Sci.*, **44**, 2341–2348.

Numaguti, A. and Y.-Y. Hayashi, 1991a: Behaviors of cumulus activity and the structures of circulations in an "aqua planet" model. Part I: The structure of super clusters. *J. Meteor. Soc. Japan*, **69**, 541–561.

Numaguti, A. and Y.-Y. Hayashi, 1991b: Behaviors of cumulus activity and the structures of circulations in an "aqua planet" model. Part II: Eastward moving planetary scale structure and the intertropical convergence zone. *J. Meteor. Soc. Japan*, **69**, 563–579.

Numaguti, A., 1992: Numerical experiments on the large scale structure of cumulus activity in the tropics. Ph.D. Thesis, University of Tokyo. (in Japanese).

Numaguti, A., 1993: Dynamics and energy balance of the Hadley circulation and the tropical precipitation zones: Significance of the distribution of evaporation. *J. Atmos. Sci.*, **50**, 1874–1887.

Ropelewski, C.F. and M.S. Halpert, 1987: Global and Regional Scale Precipitation Patterns Associated with the El Nino/Southern Oscillation *Mon. Wea. Rev.*, **115**, 1606–1626.

Spencer, R.W., 1993: Global oceanic precipitation from the MSU during 1979–91 and comparisons to other climatologies. *J. Climate*, **6**, 1301–1326.

Ting, M. and I.M. Held, 1990: The stationary wave response to a tropical SST anomaly in an idealized GCM. *J. Atmos. Sci.*, **47**, 2546–2566.

Tsuyuki, S. 1988: El Nino events and climate in the world. Lecture Notes on Long-range Forecast, September 1998, Japan Meteorological Agency, 10–16 (in Japanese).

Wang, B., 1988: Dynamics of tropical low-frequency waves: an analysis of the moist Kelvin wave. *J. Atmos. Sci.*, **45**, 2051–2065.

Wu, G.-X. and H.-Z. Liu, 1992: Atmospheric precipitation in response to equatorial and tropical sea surface temperature anomalies. *J. Atmos. Sci.*, **49**, 2236–2255.

Yano, J.-I. and K.A. Emanuel, 1991: An improved model of the equatorial troposphere and its coupling with the stratosphere. *J. Atmos. Sci.*, **48**, 377–389.

「水惑星」の赤道上に局在する暖水域が形成する熱帯の降水分布

保坂征宏
（気象庁気象研究所気候研究部）
石渡正樹
（北海道大学大学院地球環境科学研究科）
竹広真一・中島健介
（九州大学理学部地球惑星科学科）
林　祥介
（東京大学大学院数理科学研究科）

熱帯に局在する暖水域が熱帯域の大規模な降水分布に与える影響を調べるために水惑星実験を行った。用いた数値モデルは、T42L16 の分解能を持つ全球プリミティブモデルであり、簡略な水過程を含む。暖水域は、東西一様南北対称な SST 分布をもつ海洋の赤道上に置いた。

得られた熱帯域の降水分布は、暖水域の西側での降水減少と東側の広範な領域での増加、という東西非対称性の発生に特徴付けられる。その傾向は用いた積雲のパラメタリゼーション (対流調節と Kuo スキーム) によらない。西側では、中層の昇温による安定度の増加と下降流が見られ、降水の減少と整合的であった。東側では、中層の昇温はあるものの、下層での南北収束による水蒸気の増加が安定度の減少をもたらし、降水の増加と対応していた。

蒸発の評価に用いられる下層風速を固定した実験を行った結果、非対称な降水分布の生成に WISHE は重要な要因とはなっていないことが示された。